A CONSTITUTIVE MODEL FOR STRAIN-RATE DEPENDENT DUCTILE-TO-BRITTLE TRANSITION

S. FORTINO[1], J. HARTIKAINEN[1], K. KOLARI[2], R. KOUHIA[1], T. MANNINEN[1]

[1] Helsinki University of Technology, Structural Mechanics, P.O. Box 2100, FIN-02015 TKK
[2] VTT Technical Research Center of Finland, P.O. Box 1000, FIN-02044 VTT

ABSTRACT

Most materials exhibit rate-dependent inelastic behaviour. Increasing strain-rate usually increases the yield stress thus enlarging the elastic range. However, the ductility is gradually lost, and for some materials there exist a rather sharp transition strain-rate after which the material behaviour is completely brittle.

In this paper, a simple phenomenological approach to model ductile-to-brittle transition of rate-dependent solids is presented. The model is based on a consistent thermodynamic formulation using proper expressions for the Helmholtz free energy and the dissipation potential, which is additively split into damage and visco-plastic parts, and the transition behaviour is obtained through a stress dependent damage potential. In addition, the basic features of the model are discussed and a numerical example is presented.

1 INTRODUCTION

A large number of engineering materials, such as metals, polymers, concrete, soils and rock, can show reduction in the load carrying capacity accompanied by increasing localised deformations after the ultimate load is reached. If this phenomenon is considered as material property, it will lead to a negative slope of the stress-strain diagram, which is known as strain softening. In this study, a phenomenological model, which is capable to describe the strain-rate dependent ductile-to-brittle transition, is presented. The ductile behavior is considered as a viscoplastic feature, whereas the strain softening phenomenon, after reaching the transition strain-rate, is dealt with a continuum damage model.

A demerit pertaining to strain-softening models for classical continua is that they result in problems which are not well-posed in general. The field equations of motion lose hyperbolicity and become elliptic as soon as strain softening occurs. The domain is split into an elliptic part, in which the waves are not able to propagate, and into a hyperbolic part with propagating waves. In static and quasi-static problems, localisation of deformation is usually understood as a synonym to the loss of ellipticity of the underlying rate-boundary value problem. When such problems are solved numerically, the solution of the localisation zone of zero thickness can result in mesh sensitivity. A simple remedy is to include viscous effects in the plastic model as proposed in [1]. Other improvements, e.g. [2, 3, 4], are also possible. However, they usually involve additional field unknowns which make numerical computations much more time-consuming. Also, the physical interpretation of the additional boundary conditions can be ambiguous.

2 THERMODYNAMIC FORMULATION

The constitutive model is derived using a thermodynamic formulation, in which the material behaviour is described completely through the Helmholz free energy and the dissipation potential in terms of the variables of state and dissipation and considering that the Clausius-Duhem inequality is satisfied [5].

The Helmholtz free energy

$$\psi = \psi(\epsilon_{\mathrm{e}}, \omega) \tag{1}$$

is assumed to be a function of the elastic strains, ϵ_{e}, and the so-called continuity or integrity, ω. The elastic strains together with the inelastic strains, ϵ_{i}, constitute the total strains as

$$\epsilon = \epsilon_{\mathrm{e}} + \epsilon_{\mathrm{i}}. \tag{2}$$

The continuity in turn is a function of the scalar damage parameter, D, as

$$\omega = 1 - D. \tag{3}$$

It is used instead of the damage parameter to simplify the notation.

As usual in the solid mechanics, the dissipation potential

$$\varphi = \varphi(\sigma, Y) \tag{4}$$

is expressed in terms of the thermodynamic forces σ and Y dual to the fluxes $\dot{\epsilon}_{\mathrm{i}}$ and $\dot{\omega}$, respectively. The dissipation potential is associated with the power of dissipation, γ, such that

$$\gamma = \frac{\partial \varphi}{\partial \sigma} : \sigma + \frac{\partial \varphi}{\partial Y} Y. \tag{5}$$

Convexity is not a prerequisite for the dissipation potential but the condition that the product $(\partial\varphi/\partial\sigma) : \sigma + (\partial\varphi/\partial Y)Y$ is non-negative.

The Clausius-Duhem inequality, in the absence of thermal effects, is formulated as

$$\gamma \geq 0, \quad \gamma = -\rho\dot{\psi} + \sigma : \dot{\epsilon}, \tag{6}$$

where ρ is the material density. Using definitions (2) and (5) and defining that $\partial\psi/\partial\omega = Y$, inequality (6) can be reformulated as

$$\left(\sigma - \rho\frac{\partial \psi}{\partial \epsilon_{\mathrm{e}}}\right) : \dot{\epsilon}_{\mathrm{e}} + \left(\dot{\epsilon}_{\mathrm{i}} - \frac{\partial \varphi}{\partial \sigma}\right) : \sigma + \left(-\dot{\omega} - \frac{\partial \varphi}{\partial Y}\right) Y = 0. \tag{7}$$

Then, if eq. (7) holds for any evolution of $\dot{\epsilon}_{\mathrm{e}}$, σ and Y, inequality (6) is satisfied and the following relevant constitutive relations are obtained:

$$\sigma = \rho\frac{\partial \psi}{\partial \epsilon_{\mathrm{e}}}, \qquad \dot{\epsilon}_{\mathrm{i}} = \frac{\partial \varphi}{\partial \sigma}, \qquad \dot{\omega} = -\frac{\partial \varphi}{\partial Y}. \tag{8}$$

3 PARTICULAR MODEL

A particular expression for the free energy, describing the elastic material behaviour with the reduction effect due to damage, is given by

$$\rho\psi = \frac{1}{2}\omega\epsilon_{\mathrm{e}} : C_{\mathrm{e}} : \epsilon_{\mathrm{e}} \tag{9}$$

where C_{e} is the elasticity tensor.

To model the ductile-to-brittle transition due to increasing strain-rate, the dissipation potential is decomposed into the brittle damaging part, φ_{d}, and the ductile viscoplastic part, φ_{vp}, as

$$\varphi(\sigma, Y) = \varphi_{\mathrm{d}}(Y)\varphi_{\mathrm{tr}}(\sigma) + \varphi_{\mathrm{vp}}(\sigma), \tag{10}$$

where the transition function, φ_{tr}, deals with the change in the mode of deformation when the strain-rate $\dot{\epsilon}_{\mathrm{i}}$ increases. Applying an overstress type of viscoplasticity [6, 7, 8] and the principle of strain equivalence [9, 10], the following choices are made to characterize the inelastic material behaviour:

$$\varphi_{\mathrm{d}} = \frac{1}{r+1}\frac{Y_{\mathrm{r}}}{\tau_{\mathrm{d}}\omega}\left(\frac{Y}{Y_{\mathrm{r}}}\right)^{r+1}, \tag{11}$$

$$\varphi_{\mathrm{tr}} = \frac{1}{pn}\left[\frac{1}{\tau_{\mathrm{vp}}\eta}\left(\frac{\bar{\sigma}}{\omega\sigma_{\mathrm{r}}}\right)^{p}\right]^{n}, \tag{12}$$

$$\varphi_{\mathrm{vp}} = \frac{1}{p+1}\frac{\sigma_{\mathrm{r}}}{\tau_{\mathrm{vp}}}\left(\frac{\bar{\sigma}}{\omega\sigma_{\mathrm{r}}}\right)^{p+1}, \tag{13}$$

where parameters τ_{d}, r and n are associated with the damage evolution, and parameters τ_{vp} and p with the visco-plastic flow. In addition, η denotes the inelastic transition strain-rate. The relaxation times τ_{d} and τ_{vp} have the dimension of time and the exponents $r, p \geq 0$ and $n \geq 1$ are dimensionless. $\bar{\sigma}$ is a scalar function of stress, e.g. the effective stress $\sigma_{\mathrm{eff}} = \sqrt{3J_2}$, where J_2 is the second invariant of the deviatoric stress. The reference values Y_{r} and σ_{r} can be chosen arbitrarily, and they are used to make the expressions dimensionally reasonable. Since only isotropic elasticity is considered, the reference value Y_{r} has been chosen as $Y_{\mathrm{r}} = \sigma_{\mathrm{r}}^2/E$, where E is the Young's modulus.

Making use of eqs. (2) and (8), choices (9)-(13) yield the following constitutive equations:

$$\sigma = \omega C_{\mathrm{e}} : (\epsilon - \epsilon_{\mathrm{i}}), \tag{14}$$

$$\dot{\epsilon}_{\mathrm{i}} = \left[\frac{\varphi_{\mathrm{d}}}{(\tau_{\mathrm{vp}}\eta)^n \omega\sigma_{\mathrm{r}}}\left(\frac{\bar{\sigma}}{\omega\sigma_{\mathrm{r}}}\right)^{np-1} + \frac{1}{\tau_{\mathrm{vp}}\omega}\left(\frac{\bar{\sigma}}{\omega\sigma_{\mathrm{r}}}\right)^{p}\right]\frac{\partial\bar{\sigma}}{\partial\sigma}, \tag{15}$$

$$\dot{\omega} = -\frac{\varphi_{\mathrm{tr}}}{\tau_{\mathrm{d}}\omega}\left(\frac{Y}{Y_{\mathrm{r}}}\right)^{r}. \tag{16}$$

Moreover,

$$Y = \rho\frac{\partial\psi}{\partial\omega} = \frac{1}{2}(\epsilon - \epsilon_{\mathrm{i}}) : C_{\mathrm{e}} : (\epsilon - \epsilon_{\mathrm{i}}) = \frac{1}{2\omega^2}\sigma : C_{\mathrm{e}}^{-1} : \sigma. \tag{17}$$

This particular model has the following general properties:

- Elastic stiffness is reduced monotonously due to damage (eq. (14));
- The model does not include any specific yield stress;
- In the absence of damage evolution, the inelastic model (15) behaves under a constant uniaxial strain-rate loading as

  $$\sigma \to (\tau_{\mathrm{vp}}\dot{\epsilon}_0)^{1/p}\sigma_{\mathrm{r}} \quad \text{when} \quad t \to \infty,$$

  where $\dot{\epsilon}_0$ is a prescribed strain-rate;
- In the evolution of damage based on eq. (16), the constraint for the continuity ω that $\omega \in [0, 1]$ is satisfied automatically, since $\omega(x, 0) = 1$, $\dot{\omega} \leq 0$ and $\dot{\omega} \to 0$ as $\omega \to 0$;

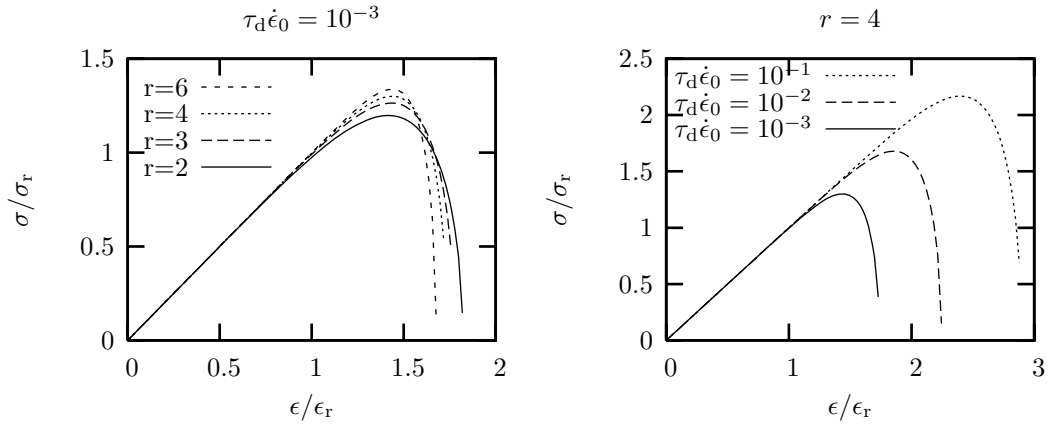

Figure 1: Uniaxial constant strain-rate loading for elastic material with damage.

- The transition function $\varphi_{\rm tr}$ in eq. (16) deals with the change in the mode of deformation through the damage evolution such that

$$\varphi_{\rm tr} \geq 0 \quad \text{and} \quad \varphi_{\rm tr} \approx 0 \text{ when } \|\dot{\epsilon}_{\rm i}\| < \eta \quad \text{and} \quad \varphi_{\rm tr} > 1 \text{ when } \|\dot{\epsilon}_{\rm i}\| > \eta;$$

- Inequality (6) is satisfied *a priori* for any admissible isothermal process. Moreover, the dissipation potential (10) is a non-convex function with respect to the thermodynamic forces σ and Y.

The sensitivity of the material parameters on the damage evolution is studied next for constant strain-rate loading ($\epsilon = \dot{\epsilon}_0 t$). First, the behaviour of the pure damage model, i.e. when $\epsilon_{\rm i} \equiv 0$ and $\varphi_{\rm tr} \equiv 1$, is shown in fig. 1 for varying relaxation time $\tau_{\rm d}$ and exponent r. In this case the solution can be obtained in the closed form

$$\frac{\sigma}{\sigma_{\rm r}} = \sqrt{1 - \left(\frac{1}{2}\right)^r \frac{2}{2r+1} \frac{\epsilon_{\rm r}}{\tau_{\rm d}\dot{\epsilon}_0} \left(\frac{\epsilon}{\epsilon_{\rm r}}\right)^{2r+1}} \left(\frac{\epsilon}{\epsilon_{\rm r}}\right), \tag{18}$$

where the reference strain is defined as $\epsilon_{\rm r} = \sigma_{\rm r}/E$.

For the full model the strain rate $\dot{\epsilon}_0$ is varied on both sides of the transition strain-rate η. Both exponents p and r have the value of 4 and the visco-plastic relaxation time $\tau_{\rm vp}$ is set to η^{-1} in all cases shown in fig. 2.

Figure 2a shows the stress-strain behaviour for varying damage relaxation times $\tau_{\rm d}$, as $\tau_{\rm d}\eta = 10^{-5},\ 10^{-3}$ and 10^{-2}, and strain rates $\dot{\epsilon}_0$, as $\dot{\epsilon}_0/\eta = 0.1$, 1 and 10, considering that $n = 4$. For the lowest strain rate $\dot{\epsilon} = \eta/10$ all the curves coincide. At the loading rate equal to the transition strain rate, the results for $\tau_{\rm d} = 10^{-2}\eta^{-1}$ and $10^{-3}\eta^{-1}$ are indistinguishable. As it can be expected, the difference is largest for the fastest loading rates and the deepest strain softening is obtained for the smallest relaxation time $\tau_{\rm d} = 10^{-5}\eta^{-1}$.

The effect of the transition function exponent n is studied in fig. 2b for the fastest loading rate $\dot{\epsilon} = 10\eta$ and considering that $\tau_{\rm d} = 10^{-3}\eta^{-1}$. The model seems to be relatively insensitive to the value of the exponent in the power law type of transition function.

The evolution of damage and its thermodynamic conjugate force for the fastest loading rate and varying damage relaxation times are shown in figs. 2c and 2d, respectively. As it can be seen from fig. 2c, largest damage occurs for the smallest values of $\tau_{\rm d}$.

In figs. 2e and 2f the inelastic strain and strain-rate are shown for $\tau_{\rm d}\eta = 10^{-3}$ and different loading rates. Observe that $\dot{\epsilon}_{\rm i} > \dot{\epsilon}_0$ for the fastest loading in the softening region.

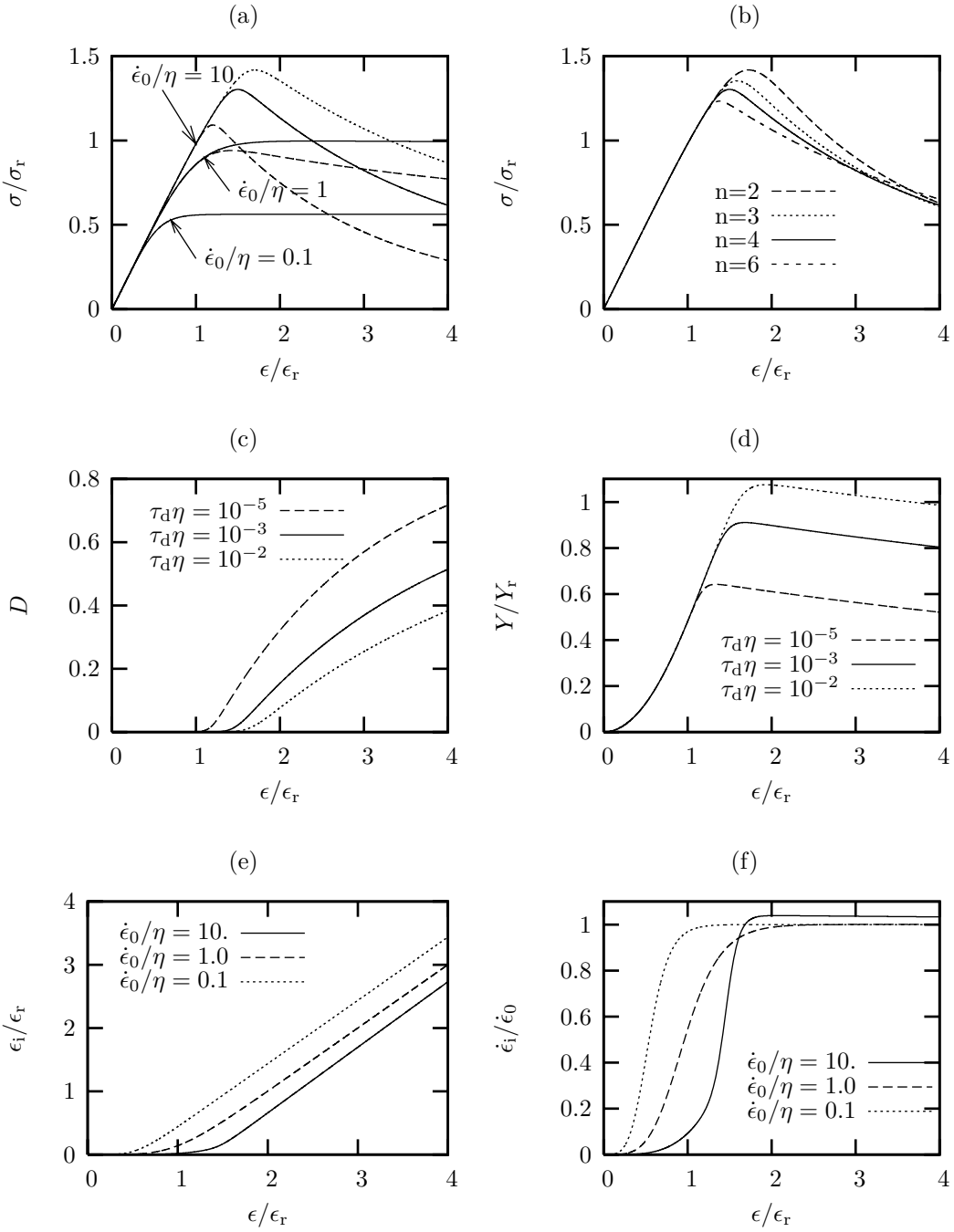

Figure 2: Uniaxial constant strain-rate loading. The line types in (a) equal to those in (c) and (d).

4 ALGORITHMIC TREATMENT

For rate-dependent solids implicit time integrators are preferable. In this study, the backward Euler scheme is used to integrate the constitutive model at the integration point level. Although the backward Euler scheme is asymptotically only first order accurate, it has good accuracy properties for large, practically relevant time-steps [11].

The constitutive model (14)-(16) is rewritten using matrix notation in the form

$$\dot{\boldsymbol{\sigma}} = \mathbf{f}_\sigma(\boldsymbol{\sigma}, \omega), \tag{19}$$

$$\dot{\omega} = f_\omega(\boldsymbol{\sigma}, \omega) \tag{20}$$

such that

$$\mathbf{f}_\sigma(\boldsymbol{\sigma}, \omega) = \omega \mathbf{C}_\mathrm{e}(\dot{\boldsymbol{\epsilon}} - \dot{\boldsymbol{\epsilon}}_\mathrm{i}) + \frac{f_\omega}{\omega}\boldsymbol{\sigma}, \tag{21}$$

$$f_\omega(\boldsymbol{\sigma}, \omega) = -\frac{\varphi_\mathrm{tr}}{\tau_\mathrm{d}\omega}\left(\frac{Y}{Y_\mathrm{r}}\right)^r, \tag{22}$$

where

$$\dot{\boldsymbol{\epsilon}}_\mathrm{i} = \left[\frac{\varphi_\mathrm{d}}{(\tau_\mathrm{vp}\eta)^n \omega \sigma_\mathrm{r}}\left(\frac{\bar{\sigma}}{\omega\sigma_\mathrm{r}}\right)^{np-1} + \frac{1}{\tau_\mathrm{vp}\omega}\left(\frac{\bar{\sigma}}{\omega\sigma_\mathrm{r}}\right)^p\right]\frac{\partial\bar{\sigma}}{\partial\boldsymbol{\sigma}}, \tag{23}$$

$$Y = \frac{1}{2\omega^2}\boldsymbol{\sigma} : \mathbf{C}_\mathrm{e}^{-1} : \boldsymbol{\sigma}. \tag{24}$$

Applying the backward Euler scheme and the Newton's linearisation method to the evolution equations (19) and (20) results in the linear system of equations[1]

$$\begin{bmatrix} \mathbf{H}_{11} & \mathbf{h}_{12} \\ \mathbf{h}_{21}^T & H_{22} \end{bmatrix}\begin{Bmatrix} \delta\boldsymbol{\sigma} \\ \delta\omega \end{Bmatrix} = \Delta t \begin{Bmatrix} \mathbf{f}_\sigma \\ f_\omega \end{Bmatrix} - \begin{Bmatrix} \Delta\boldsymbol{\sigma} \\ \Delta\omega \end{Bmatrix}, \tag{25}$$

where

$$\mathbf{H}_{11} = \mathbf{I} - \Delta t \frac{\partial \mathbf{f}_\sigma}{\partial \boldsymbol{\sigma}}, \tag{26}$$

$$\mathbf{h}_{12} = -\Delta t \frac{\partial \mathbf{f}_\sigma}{\partial \omega}, \tag{27}$$

$$\mathbf{h}_{21}^T = -\Delta t \frac{\partial f_\omega}{\partial \boldsymbol{\sigma}}, \tag{28}$$

$$H_{22} = 1 - \Delta t \frac{\partial f_\omega}{\partial \omega}. \tag{29}$$

The algorithmic tangent matrix, i.e. the Jacobian of the algorithmic stress-strain relation has the simple form

$$\mathbf{C} = \omega \widetilde{\mathbf{H}}_{11}^{-1}\mathbf{C}_\mathrm{e}, \tag{30}$$

where

$$\widetilde{\mathbf{H}}_{11} = \mathbf{H}_{11} - \mathbf{h}_{12}H_{22}^{-1}\mathbf{h}_{21}^T. \tag{31}$$

As it can be seen, the Jacobian matrix is in general nonsymmetric due to the damage. The algorithmic tangent matrix is a necessity for the Newton's method to obtain asymptotically quadratic convergence of the global equilibrium iterations.

[1]The symbols Δ and δ refer to incremental and iterative values, $\boldsymbol{\sigma}_n^{i+1} = \boldsymbol{\sigma}_n^i + \delta\boldsymbol{\sigma}_n^i$, $\Delta\boldsymbol{\sigma}_n^i = \boldsymbol{\sigma}_n^i - \boldsymbol{\sigma}_{n-1}$, where the sub- and superscripts refer to step- and iteration numbers, respectively.

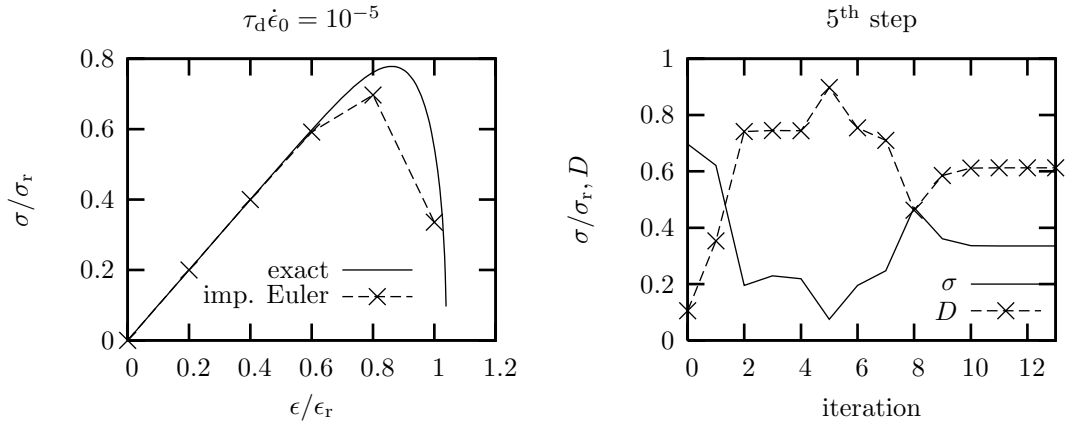

Figure 3: Instability in the implicit backward Euler scheme.

Although the backward Euler scheme is simple and gives accurate results in visco-plastic computations for large time-steps, in the case of damage the scheme can generate oscillations which destroy the convergence of the local Newton's process. This can be seen clearly, when only elastic-damaging material is considered. Applying the backward Euler scheme to a uniaxial case with pure damage evolution

$$\dot{\omega} = f_\omega(\omega) = -\frac{1}{\tau_{\rm d}\omega}\left(\frac{Y}{Y_{\rm r}}\right)^r \tag{32}$$

yields the iteration process

$$\omega_n^{i+1} = \omega_n^i + \frac{\Delta t f_\omega(\omega_n^i) - \Delta\omega_n^i}{1 - \Delta t f_{\omega,\omega}(\omega_n^i)}, \tag{33}$$

where the denominator is similar to the element H_{22} in eq. (25). When the denominator is negative, oscillations occur, so that the size of time-step Δt needs to be restricted. The derivative $f_{\omega,\omega}$ is

$$f_{\omega,\omega} = \frac{\partial f_\omega}{\partial\omega} = \frac{1}{\tau_{\rm d}\omega^2}\left(\frac{Y}{Y_{\rm r}}\right)^r, \tag{34}$$

and the requirement, $1 - \Delta t f_{\omega,\omega} > 0$, results in the following restriction on the time-step:

$$\frac{\Delta t}{\tau_{\rm d}} < 2^r\omega^2\left(\frac{\epsilon_{\rm r}}{\epsilon}\right)^{2r}. \tag{35}$$

The oscillations are illustrated in fig. 3, in which the analytical stress-strain curve together with the numerical solution using the implicit backward Euler scheme are shown on the left, and the iteration histories of stress and damage for the fifth step ($\epsilon/\epsilon_{\rm r} \in (0.8, 1.0)$) on the right. The following parameters have been used: $r = 4$, $\tau_{\rm d} = 10^{-2}$ s, $\dot{\epsilon}_0 = 10^{-3}$ s^{-1} and $Y_{\rm r} = 0.01$ ($E = 40$ GPa, $\sigma_{\rm r} = 20$ MPa). Moreover, $\Delta t = 0.1$ s. At the fifth step, the term H_{22} becomes negative and the domain of attraction of the Newton process is reached not until after eight iterations.

5 NUMERICAL EXAMPLE

A compressed specimen ($(x, y, z) \in \Omega = (0, L) \times (0, B) \times (0, H)$, $L = 200$ mm, $B = 100$ mm, $H = 1$ mm) is analysed under plane strain condition, as shown in fig. 4.

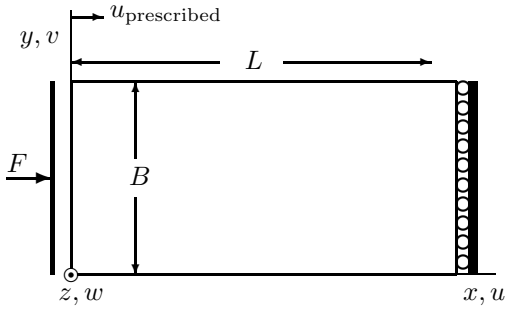

Figure 4: Problem description.

A strain localisation into a shear band is expected to take place due to damage induced strain-softening. The horizontal displacement at the left-hand side edge is prescribed at constant rate $\dot{u}_{\text{prescibed}}$ and constrained to remain straight. A von-Mises type viscoplastic solid is used, i.e. $\bar{\sigma} = \sigma_{\text{eff}}$. The constitutive parameters have the following values: Young's modulus $E = 40$ GPa, Poisson's ratio $\nu = 0.3$, reference stress $\sigma_{\text{r}} = 20$ MPa, the viscoplastic relaxation time $\tau_{\text{vp}} = 1000$ s, the transition strain rate $\eta = 10^{-3}$ s^{-1}. All the exponents p, r and n have the value of 4.

Eight-node-trilinear elements with mean dilatation formulation [12] were used in the computations, which were carried out for two different meshes, a coarse mesh of 12×6 elements and a finer mesh of 48×24 elements. To trigger the unstable localisation, an imperfection via a patch of elements was introduced by reducing the reference stress by 5 %.

Figure 5 shows the load-displacement curves calculated for three different loading rates (on the upper left) and four different damage relaxation times (on the upper right) using the coarse mesh, and for both meshes considering that $\tau_{\text{d}}\eta = 10^{-3}$ and $\dot{\epsilon}_0/\eta = 10$ (at the bottom). The average strain rate is defined as $\dot{\epsilon}_0 = \dot{u}_{\text{prescribed}}/L$. In comparison to the results of pure material behaviour (fig. 2a), the softening behaviour of the structure is much more rapid due to the localisation band.

As explained in the preceding section, a large number of time-step reductions, due to diminished convergence of local iterations, had to be done during the computations, especially in the computations for the highest loading rate.

Damage distribution is shown in fig. 6. It can be observed that damage bands are approximately at ±45° angles as in the classical strain-softening von-Mises type elastoplasticity.

6 CONCLUDING REMARKS

A phenomenological constitutive model for modelling the ductile-to-brittle transition due to increased strain-rate is presented. In the present model, the dissipation potential is additively split into damage and visco-plastic parts and the transition behaviour is obtained using a stress dependent damage potential. In this preliminary study, only isotropic damage and von-Mises type viscoplastic flow are considered. However, the chosen approach allows easily an extension to more advanced damage models. Further investigations will be focused on the study of material length scale.

The numerical implementation is also discussed. Due to the unstable nature of damage,

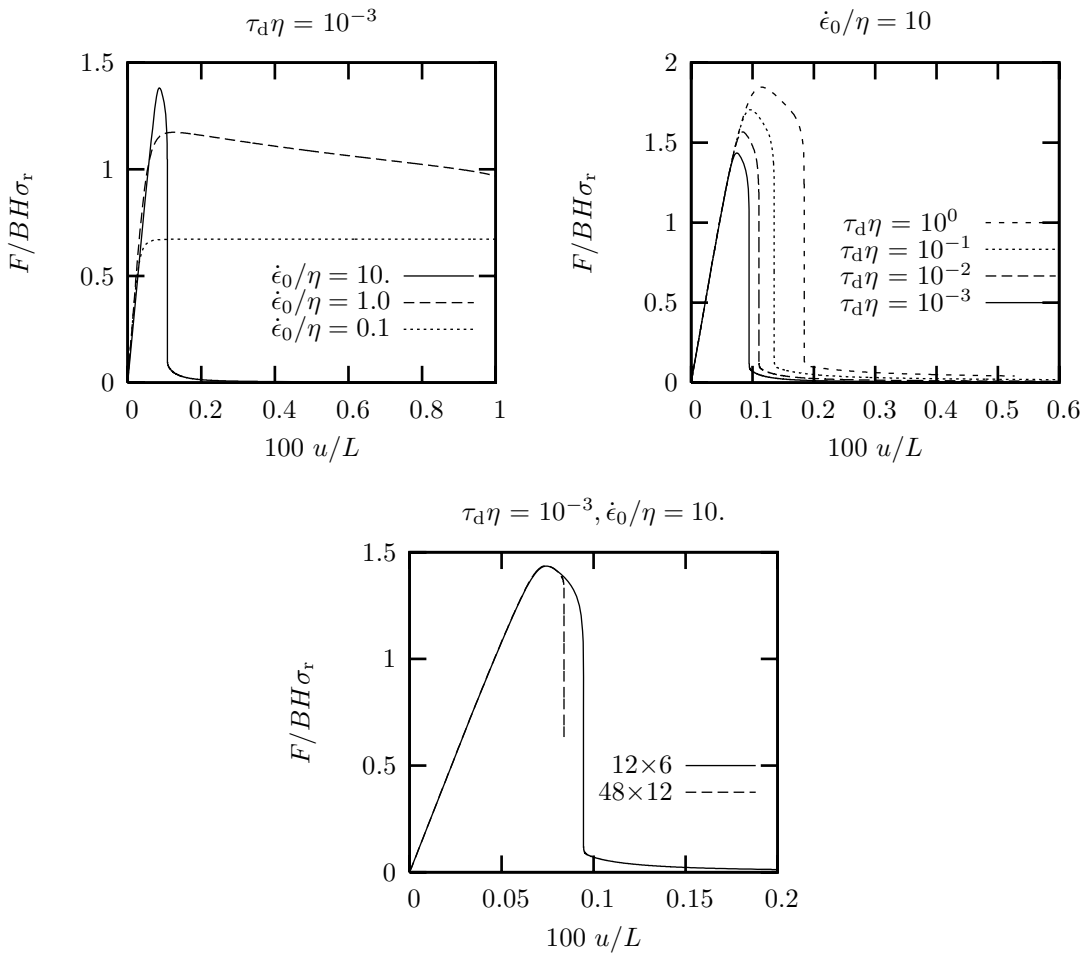

Figure 5: Load-displacement curves. A mesh of 12×6 elements in the upper figures.

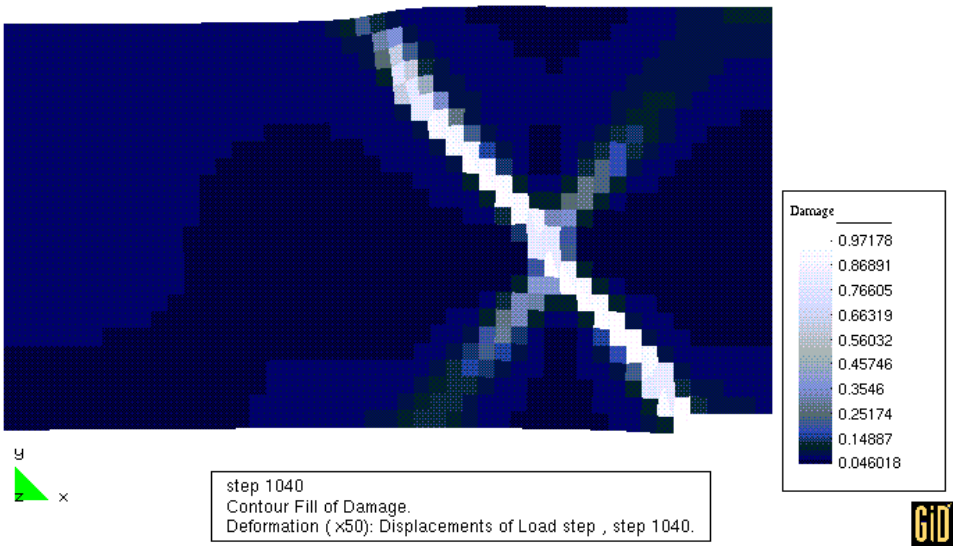

Figure 6: Damage D distribution for $\dot{\epsilon} = 10\eta$ and $\tau_{\rm d}\eta = 10^{-3}$ at the end of the computation ($F = 0.618BH\sigma_{\rm r}$). A mesh of 48×24 elements. Displacements magnified by 50 times.

the conventional backward Euler method does not perform well. Oscillations in the damage variable can result in convergence problems in the local Newton iteration at the integration point level. Therefore, further studies will be directed to develop a robust integration scheme for damage evolution.

ACKNOWLEDGMENTS

This research has been supported in part by Tekes - the National Technology Agency of Finland (project KOMASI, decision number 40288/05) and in part by the Academy of Finland, (decision number 210622).

REFERENCES

[1] A. Needleman. *Material rate dependence and mesh sensitivity in localization problems*, Comp. Meth. Appl. Mech. Engng., **67**, 69–85 (1988).

[2] A.C. Eringen. *Microcontinuum Field Theories, I. Foundations and Solids*, Springer, New-York, 1999.

[3] L.J. Sluys. *Wawe propagation, localisation and dispersion in softening solids*, PhD thesis, Department of Civil Engineering, Delft University of Technology, 1992.

[4] W. Wang. *Stationary and propagative instabilities in metals – a computational point of view*, PhD thesis, Department of Civil Engineering, Delft University of Technology, 1997.

[5] M. Frémond. *Non-Smooth Thermomechanics*, Springer, Berlin, 2002.

[6] P. Perzyna. *Fundamental problems in viscoplasticity*, Advances in Applied Mechanics, **9**, 243–377 (1966).

[7] G. Duvaut and L.J. Lions. *Inequalities in Mechanics and Physics*, Springer, Berlin, 1972.

[8] M. Ristinmaa and N.S. Ottosen. *Consequences of dynamic yield surface in viscoplasticity*, Int. J. Solids Structures, **37**, 4601–4622 (2000).

[9] J. Lemaitre, J.-L. Chaboche. *Mechanics of Solid Materials*, Cambridge University Press, 1990.

[10] J. Lemaitre. *A Course on Damage Mechanics*, Springer-Verlag, Berlin, 1992.

[11] R. Kouhia, P. Marjamäki, J. Kivilahti. *On the implicit integration of rate-dependent inelastic constitutive models*, Int. J. Numer. Meth. Engng., **62**, 1832–1856 (2005).

[12] T.J.R. Hughes. *The Finite Element Method - Linear Static and Dynamic Finite Element Analysis*, Prentice-Hall, 1987.